Fluorine and sodium depletion followed by refractive index modification imprinted on fluorophosphate glass surface by thermal poling

Gustavo Galleani, Alain Abou Khalil, Lionel Canioni, Marc Dussauze, Evelyne Fargin, Thierry Cardinal, Andrea S.S. de Camargo

Fluorine and sodium depletion followed by refractive index modification imprinted on fluorophosphate glass surface by thermal poling.

Gustavo Galleani[1,4*], Alain Abou Khalil[2], Lionel Canioni[2], Marc Dussauze[3], Evelyne Fargin[4], Thierry Cardinal[4*] and Andrea S. S. de Camargo[1]

[1] *Sao Carlos Institute of physics – University of Sao Paulo – Sao Carlos-SP, Brazil*

[2] *Univ. Bordeaux, CNRS, CEA, CELIA, UMR 5798, F-33400 Talence, France*

[3] *Univ. Bordeaux, ISM, UMR 5255, F-33405 Talence, France*

4 Univ. Bordeaux, CNRS, ICMCB, UMR 5026, F-33608 Pessac, France

[1] Corresponding authors: E-mail: gugalleani@yahoo.com.br
E-mail: thierry.cardinal@icmcb.cnrs.fr

ABSTRACT

Thermal poling using microstructured electrodes on oxyfluoride glasses have been investigated and the impact on optical properties is evaluated. A micrometer refractive index modification based on the sodium and fluorine migration have been evidenced, creating a layer with different chemical composition compared to the original glass. Topological and optical properties modifications after poling treatment are discussed. For the first time, we described the migration of negative fluorine ion in the direction of the cathode from the glass network. Na and F migration led to a layer richer in oxides with a strong contrast of + 0.06 of the refractive index in the imprinted structures.

Keywords: glass; thermal poling; fluorophosphate; refractive index modification

1. INTRODUCTION

Thermal poling is a very powerful technique for local modification of optical, electrical and chemical properties in glass surface.[1] It comprises in employing a dc electric field below the glass transition temperature (Tg) and cooling the glass before removing the dc bias developing an increase of mobility of charge carriers, mainly alkali and alkaline-earth cations [2–6] and also some anionic

species, as first considered in 1963 by Von Hippel et al, [7] being responsible for the creation of a expended layer of few hundred of nanometers up to several micrometers depending on the experimental parameters.[8] This process induces at the anode side depletion of cations, structural reorganization,[9,10] change of the surface reactivity,[11,12] wettability and modification in surface potential,[13] modifications of the index and induced second-order nonlinear response (change in optical properties).[14,15] Surface patterning of those modifications have been recently demonstrated using structured electrodes.[16,17]

Indeed, glasses treated by thermal poling have prominent potential for applications in materials with multiple functionalities as photonic integrated circuits for instance. Looking more specifically to the modifications of the optical properties, it is in consequence possible to develop in a glass by thermal poling, arrays of microlenses, micro-optic devices such as waveguides and diffraction gratings[18]. The patterning of these modifications can be done using structured electrodes that act like stamps to control the surface properties in the micrometer scale, paving the way for design of these functional elements.[19]

Upon thermal poling, mobile ions present in the glass composition drift to the cathode, resulting in a sodium depleted zone on the anodic side. In most glass compositions described in the literature, the mobility of sodium cations and oxygen are the main drifted species responsible for the compositional changes, even if the thermal poling is also reported to promote migration of bigger alkalis, such as potassium or alkaline earth ions such as calcium but in a less extent.[20] Hence, the resulting poled layer is mainly composed by the network-former compounds and shows different chemical and physical surface properties as compared to the original glass. Thermal poling effect has been substantially studied in several oxide glasses such as silica glass[21], silicates[22,23], phosphates[24], tellurides[25,26], heavy metal oxides[10], as well as chalcogenide glasses. [27,28] These works have assisted to better understand the mechanism happening in the development of properties in different kind of glasses. The atomic structure of the glass adjusts the compositional changes that take places during the treatment by poling, rearranging the “parent” glass structure with local coordination changes, condensation reactions and injecting protons or other counter-ions to maintain the charge-balance requirements to the glass network.

On the other way, oxyfluoride glasses have not been yet used, to the best of our knowledge, as materials in thermal poling. The role of conductive fluorine ions migration in the optical and structural properties is still unknown and could be explored to promote great changes in glass properties. One promising system is the use of fluorophosphate glasses as host for the development of optical devices from thermal poling. They offer the promise of emerging the profitable optical properties of fluoride with the advantageous mechanical properties of oxide glasses. They have been extensively described

in literature for photonic applications, taking its optical properties advantages.[29,30]

In this context, the aim of this work is on engineering fluorophosphate glass material to tailor their optical properties upon thermal poling. The migration of not only cationic species, but also fluorine upon poling treatment is explored and the impact on the glass surface property and structure is investigated. A particular attention is targeted on the impact of the thermal poling using a micro-structured electrode on the refractive index modification.

2. EXPERIMENTAL PROCEDURE

Oxyfluoride vitreous sample with the molar composition $50Na(PO_3)_2–20GdF_3–20BaF_2–10CaF_2$ (mol %), labelled as NPGF, was prepared by the conventional melt-quenching method. To avoid fluorine losses, powder precursors were mixed and melted at 950 ℃ in a capped platinum crucible in an electric furnace for 20 min. Finally, the melted glass was cooled rapidly in a brass mold kept at 20 ℃ below the glass transition temperature (Tg = 290 ºC) and kept in a resistive oven for 4 h to remove residual stresses.

Prior poling, the glass transition temperature was determined by differential scanning calorimetric (DSC) measurements performed using a TA Instruments 2910 calorimeter at a heating rate of 10℃.min^{-1} and placing glass pieces of around 20 mg into the Al pans under nitrogen atmosphere and Raman measurements were done on a spectrometer HR800 (Horiba/Jobin Yvon) in backscattering mode using a continuous laser operating at 532 nm was used.

Thermal poling was then performed under a N_2 flow of 6 L/min. Polished glass sample was heated at 250 ℃ and the DC voltage was raised to 1.2 kV with a 350 V/min rate and left at these conditions for 30 min. The glass was then cooled down to room temperature before removing the dc bias. The anode consisted of a home-prepared patterned ITO electrode facing the sample. In the present work, they were made by laser ablation of a 100 nm thick indium tin oxide (ITO) layer (8-12 Ω sq^{-1}) deposited on a microscope glass slide using a nanosecond YAG laser source at 1064 nm with a scanning speed of 1000 mm/s at pulse energy of 150 μJ. The pattern was inscribed on the electrode placed on a microscope stage controlled by a software. The final ITO coated microscope slide was then composed of alternating conductive and nonconductive areas. After structured, the ITO free side of the electrode was covered by a gold conductive thin film to ensure conductivity. A piece of silicon wafer was used on the cathode side, and a soda lime glass was used in the middle of the silicon and the sample to avoid reduction of the sample at the cathode.

Secondary ion mass-spectrometry (SIMS) evaluations were performed on a PHI Adept 1010 dynamic SIMS system. Excitation of secondary ion emission was made by a focused primary ion beam

of Cs^+ at 2 KeV. For the negative secondary ions, sample was biased to - 30 keV and for positive ions + 30 kV. A qualitative distribution of elements in poled sample was examined by etching of the surface with ion beam. An area of 300 x 300 μm^2 was scanned. Etching rate was obtained from the profundity of the crater measured by optical profilometry

Infrared reflectance spectra were recorded in reflection mode prior and after poling treatment to achieve details on the structural modifications related with the charge migrations in a Vertex 70V spectrometer in a primary vacuum. The equipment is equipped with a deuterated triglycine sulfate detector, a globar type source and a mid/far infrared range beam splitter. Kramers-Krönig analysis were used to calculate the absorbance spectra from these spectra.[31]

Atomic Force Microscopy (AFM) measurements were performed at the samples by an AFM Dimensions Icon (Bruker) using a PFQNE-AL cantilever.

The refractive index change Δn was evaluated using a commercial quantitative phase imaging QWLSI sensor, SID4Bio by PHASICS in transmission mode placed on a microscope. An intensity image and a phase image showing the optical path difference (OPD) produced by the transmitted light is the final output of the wave front sensor.

3. RESULTS AND DISCUSSION

3.1. Bulk glass characterization

The oxyfluoride vitreous sample $50NaPO_3$-$20GdF_3$-$20BaF_2$-$10CaF_2$ obtained using classical melt quench technique and the thermal properties were analyzed by DSC and is shown in Figure 1. The sample exhibit a glass transition temperature (Tg) of 290 ℃ obtained from the onset point of the DSC curve and an onset crystallization temperature (Tx) of 380 ℃. The thermal stability against crystallization corresponding to the temperature difference between Tg and Tx is ΔT = 90 ℃, high enough to obtain large pieces of glasses suitable for the thermoelectrical polarization investigation.

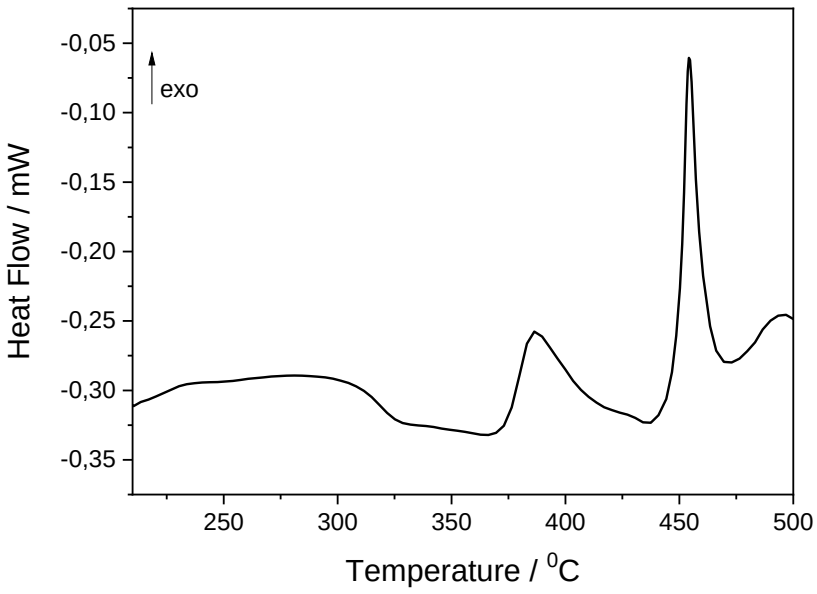

Figure 1. DSC curve of the oxyfluoride NPGF glass.

The refractive index of the NPGF glass was also measured at different wavelengths, 589 nm, 644 nm and 656 nm, and the values obtained are 1.539, 1.533 and 1.531, respectively. The values are in the range of other oxyfluoride glasses with similar composition exhibiting a classical wavelength refractive index dispersion.[32,33]

3.2.Thermal poling and subsequent surface topology and composition modification of the poled glass.

Prior to imprinting, an ITO patterned electrode has been prepared. An illustrative representation of the prepared electrode is depicted in Figure 2. After laser irradiation, electrode structuring simply consisted of a 1 cm^2 surface area, which half of the electrode was non-structured (in yellow in the figure 2, with conductive area) for macroscopic measurements, and the other half consists of structures of 30 µm x 30 µm of ablated square (white in the figure 2), distanced by 10 µm conductive lines. The structured electrode is then used as “stamps” during the imprinting poling process.

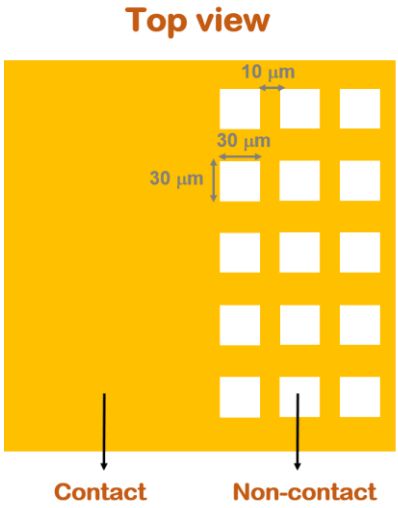

Figure 2. Schematic representation of the patterned electrode used in this work. The contact and non-contact zones are represented in yellow and white, respectively.

The thermal poling was then performed under nitrogen at 250 ℃ and 1.2 kV to avoid proton injection. After 30 minutes of poling, the glass sample was cooled to 25 ℃ and the initial applied electric field removed. Figure 3a shows, using white light microscopy, that the structured pattern was faithfully transposed to the glass poled surface by leaving a clear optical contrast at the surface. In Figure 3b, the degradation of the ITO electrode used as anode after the poling process was observed. This observation could give the first indication of a hypothesis of possible fluorine loss during the process within the anode side leading to the corrosion of the ITO layer, but further characterization and studies need to be done for prove such hypothesis.

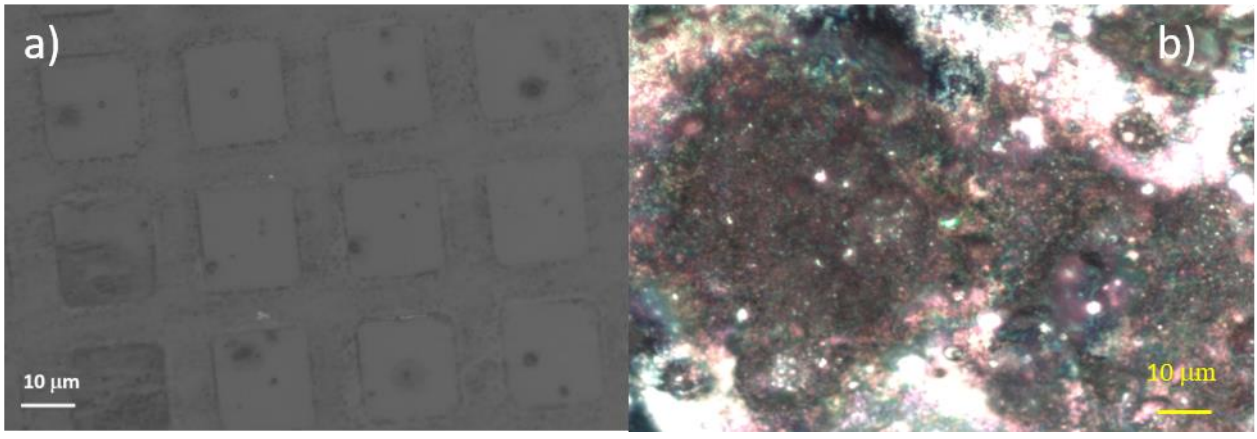

Figure 3. (a) Micrography of the surface imprinted micropattern of the NPGF glass after thermal poling treatment. (b) Microscope image of the structured electrode surface degraded after poling.

The Figure 4 evidence the changes of topology measured by AFM on imprinted area on the poled glass surface. The change of topology occurs with a surface variation around 60 nm of amplitude (Figure 4 (b)). These features appear on locations where the ITO was in electrical contact with the glass surface, known as electrostatic imprinting process of topology. [34–36] Such topology variations are linked to the migration of mobile ions after thermal poling and especially sodium ions in glasses leading to important structural rearrangements of the glass network accompanied by a density change.[11,14,36,37]

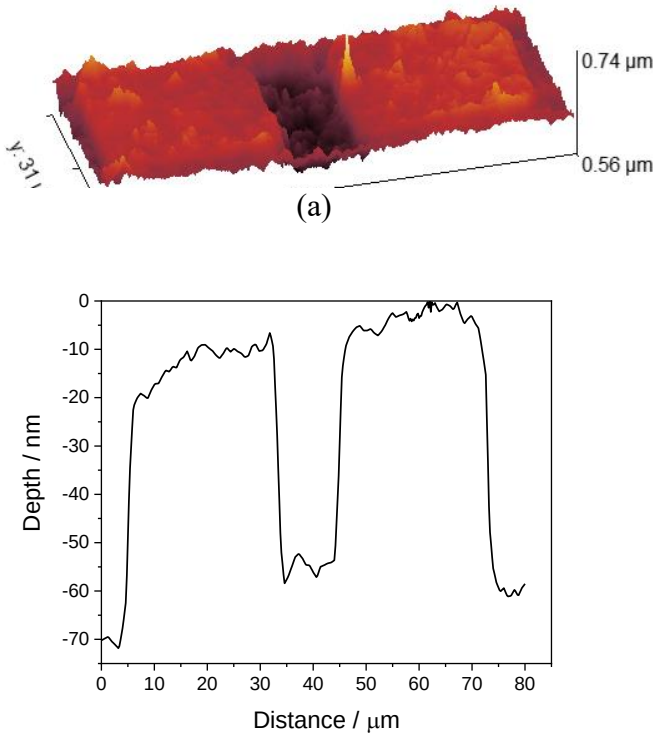

Figure 4. (a) Topology image collected by AFM and (b) profile of the NPGF glass surface after thermal poling.

Chemical composition changes were studied using SIMS on the poled oxyfluoride glass. The SIMS chemical profile of positive and negative ions distribution were collected across the non-structured part of the electrode used for the thermoelectrical process, giving access to a large poled area. The result can be seen in Figure 5.

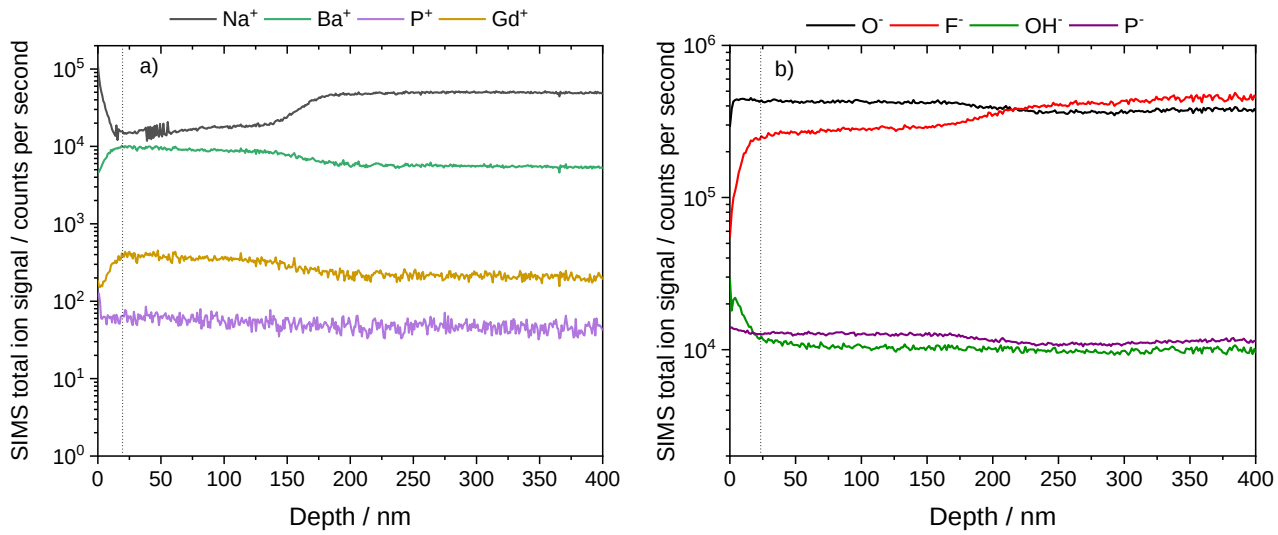

Figure 5. SIMS profile from the anode entering inside the glass for positive (a) and negative (b) ions on the NPGF oxyfluoride glass after poling treatment. The vertical dot line represents the initial point where the real trend of SIMS total ion signal can be drawn.

In Figure 5, the depth profile of positive and negative charges is inferred as counts per second signal as a function of surface depth. For both charge profile, the first few tens of seconds are because of charge distribution stabilization in the SIMS method, no real trend can be drawn up to 25 nm. The depth of the crater during the total exposure of the glass surface during the SIMS thickness has been determined at 400 nm by measuring the optical profilometry, as shown in supporting information (Figure S1). The evolution of the concentration profile of the positive species Na, Gd, P and Ba are shown in Figure 5a. One can notice that the sodium depletion occurs on a depth of about ~180 nm, assuming that the sputtering speed remains constant during the whole SIMS analysis, while the relative concentration of the Gd and Ba increases. Regarding the phosphorus cation, the profile appears constant. Concerning the anions profile shown in figure 5b, on can observe an increase of the oxygen and the phosphorus relative concentration while the proportion of fluorine decreases also on a depth about 180 nm. The relative concentration evolution of hydroxyls appears fairly constant along the whole thickness investigated. Based on the SIMS investigation, a clear depletion of sodium and fluorine is observed, which results in an increase in the relative concentration of the less mobile ions (Ba, Gd, P) which form the resulting glass network in the poled affected thickness. Based on the profile investigation, one can propose that the sodium ions have been carried along the electric field from the anode to the cathode while the fluorine anions went through the inverse route. The observed degradation of the ITO electrode after poling shown in Figure 3 is in line with such hypothesis and the attack of the ITO layer by the fluorine species. The whole process occurring during the poling is then

expected to create an oxygen enriched glass layer in the 180 nm poled region with a low concentration of fluorine anions and sodium cations inducing a possible large chemical and physical property variations.

3.3. Structural evolution of the glass after poling.

The poling procedure induces clear modification of the surface material composition on a depth up to 180 nm. Such modification is expected to produce important changes of the glass network which can be explored using IR vibrational spectroscopy.

Prior poling, Raman and Infrared spectroscopy have been conducted as reported in Figure 6a and 6b (black curve), respectively. Raman spectra of oxyfluoride phosphate glasses with similar composition ($NaPO_3$-BaF_2-YF_3) have been previously studied and the structure described in literature. [38]

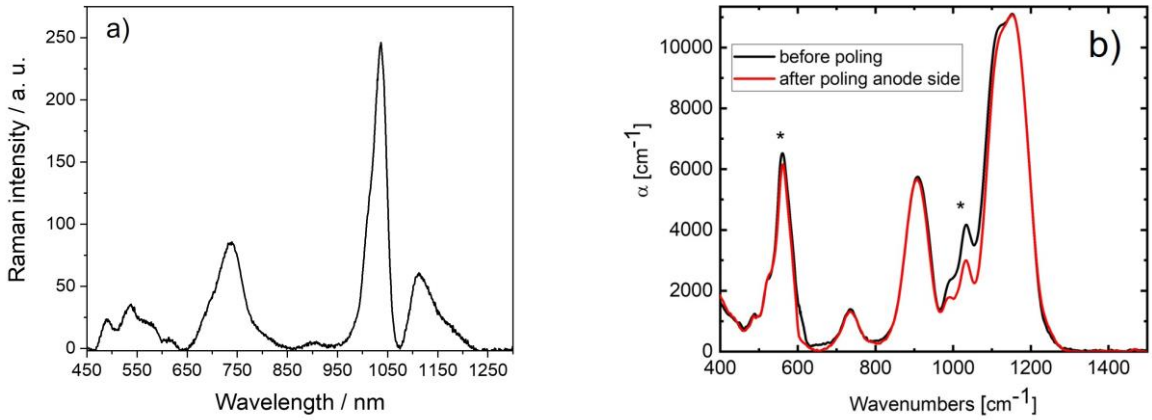

Figure 6. (a) Raman spectra of the NPGF oxyfluoride glass. (b) Comparison of absorption coefficients (α) obtained by the reflectance spectra Kramers-Kronig transformation of the NPGF glass prior (black curve) and after (red curve) poling recorded under vacuum. Asterisks highlights the positions with spectral modifications.

The Raman spectrum is formed mainly of a band at ~1040 cm^{-1} which is assigned to PO_3 symmetric stretching modes of $P_2(O,F)_7$ dimers, in $Q^{(1)}$ units, and a band at 1110 cm^{-1}, assigned to PO_2 stretching modes of metaphosphate groups. The band near 900 cm^{-1} suggest the existence of P-F bonding,[39,40] and the band observed near 740 cm^{-1} is assigned to the P-O-P symmetric stretching

mode of bridging oxygen between two phosphate tetrahedral in short chains, such as $Q^{(1)}$ species. At lower frequency, the bands in the region 450-650 cm^{-1} are typically bands of alkaline-earth bonded to fluorine species observed in pure fluoride glasses.[41] At 540 cm^{-1} i.e. the band has been assigned to NaF.[42]

Regarding the infrared spectroscopy, the bands in the region 1000-1250 cm^{-1} were assigned to $\nu_{as}PO_3^{2-}$ (PO_3F, Q^1) units, normally present at 1090 cm^{-1} for fluorophosphate glasses and $\nu_{as}PO_2^-$ ($PO_{3/2}F$, Q^2) units at 1150 cm^{-1}. At 900 cm^{-1} the band is due to ν_{asym}(POP) stretching vibration of Q^1 in chains and/or P-F bonding and at 735-745 cm^{-1} of POP ring stretching mode. At 500 cm^{-1} the band is generally to ν(POP) for phosphates,[43] while for fluoride glasses can be assigned to the stretching modes of M-F bonds.[44] Some of these network chains bring negative charges that are balanced by Na^+ charges, so it is expected modifications at these units after sodium depletion, but not only, since fluorine also due a role in these units, possibly causing modifications on it.

The structure of our NPGF glass as described by Raman above consists in the most part of Q^1 units in $P_2(O,F)_7$ dimers and the presence of some metaphosphate groups (Q^2 units). It is known that sodium ions dominantly interact with phosphate units rather than fluoride species in fluorophosphate glasses.[38,40,45] Therefore, it is reasonable to believe that sodium departures will affect mainly these phosphate units. The fluorine anions can be present in different anionic units as Gd-F, Na-F, Ba-F, but also be present in different Q^1 linked to phosphorus, forming P-F bonds, denoted as $Q^1{}_{1F}$, $Q^1{}_{2F,}$ which means one Q^1 unit having one F and two F, respectively, which has been proven to exist in previously studies by $^{19}F\{^{31}P\}$double-resonance and 2D $^{31}P\{^{19}F\}$ HMQC experiments by nuclear magnetic resonance in similar glasses, showing that F ions have bond connectivity with these phosphorus species.[38,40]

To get information about the structural modifications after poling, a comparison of absorptions obtained by IR reflectance was used. IR in reflection mode allows to probe submicron surface layer of the thermal poled sample and get information about these modifications, depicted in Figure 6b. The spectra were acquired at the anode side prior poling (in black) and after poling (in red) between 400 and 1500 cm^{-1}. The crucial region with modifications in this section is ~ 1040 cm^{-1}. One can see that thermal poling treatment induced a significant decrease of the absorption for the band ~1040 cm^{-1}, described above to belong to (FPO_3^{2-}) Q^1 units. It is assumed here that the changes are mainly connected to the Na^+ and F^- depletion layer observed by SIMS in Figure 5, which leads to the decrease of the Q^1 units. Previous report of $NaPO_3(1-x)F_x$ glasses [42] have shown a decrease in the band ~ 1040 cm^{-1} as the F content in the glass is lower. The extend of modification related to each ion is difficult at this point, since both are present at these units.

3.4. Refractive index modification by thermal poling

To better characterize the optical changes induced by the imprinted structure in the poled glass, the variation of the refractive index Δn is an essential parameter, and for that, the SID4Bio wave front sensor by PHASICS was used. The phase image of the imprinted structure in NPGF glass is shown in Figure 7a and displays a positive optical path difference (OPD) in the poled zone (darker areas in the image). The value of Δn was calculated by dividing the OPD by the thickness (l) of the imprinted region ($\Delta n = OPD/l$). Considering the thickness (l) of the poled layer determined above by SIMS and the optical profilometry (Figure S1), the qualitative value of Δn of the imprinted structures was determined. In order to evaluate the refractive index change, the surface topology (by AFM) in the poled region has been considered and compared to the phase contrast image showed in Figure 7.

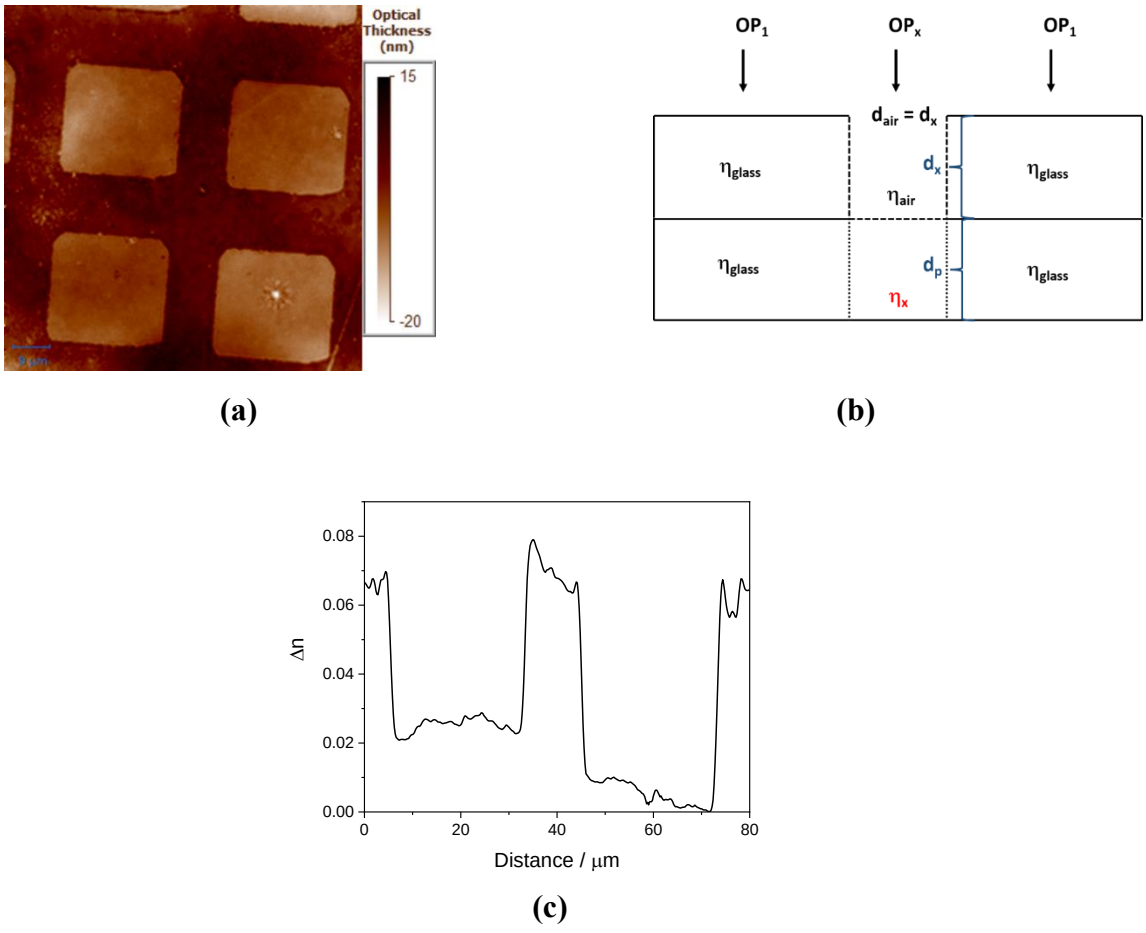

Figure 7. (a) Phase image under white light illumination of the NPGF imprinted structure after poling, (b) schematic representation of our system allowing describing refractive index and thicknesses of the different zones and in particular the zone affected by the thermal poling experiencing a contraction and (c) refractive index change (Δn) profile obtained from the phase image.

The optical path difference between the virgin glass and the zone affected by the poling treatment can be written as follow:

$$OPD = OP_x - OP_1, \quad (1)$$

$$OP_x = n_{air}.d_x + n_x . d_p, \quad (2)$$

$$OP_1 = n_{glass} . (d_p + d_x), \quad (3)$$

where n_{air} is the refractive index of air (n_{air} = 1), n_{glass} is the refractive index of our NPGF glass (n_{glass} = 1.53), d_p is the poled layer thickness determined by SIMS (180 nm), d_x is the topological change profile obtained by AFM and n_x is the refractive index of the poled layer. The OPD is the optical phase difference between the optical phase in the poled zone (OP_x) and the outside of the poled zone (OP_1)

Based on the average depth and phase contrast profile obtained for the same region of the imprinted poled glass, the refractive index profile could be obtained and the Δn profile ($\Delta n = n_x - n_{glass}$) is shown in Figure 7. A positive Δn up to ~0.06 was observed in the poled region, showing that the departure of fluorine and sodium impact the refractive index. Considering that a reduction of the sodium content should tend to decrease the refractive index, as observed in previously reported thermal poled sodium borophosphate glasses, [46] and that the fluorine departure is expected to have the opposite effect.[47]

Since the fluorine anions has much less polarizability than the oxygen, injection of fluorine in silica glass has been used to produce step-index fibers i. e., [48,49] being the fluorine responsible to decrease the refractive index. Similar approach was also responsible for refractive index decrease in phosphate glasses. [42] Therefore, in our case, as we observe fluorine departure (ejection of fluorine in the poled layer), the opposite effect is expected, so the fluorine departure observed after poling treatment is considered to be the main phenomenon driving the refractive index change in our glass.

The formation of a rich oxygen layer during poling is then definitely promoting a highest refractive index when compared to the original oxyfluoride glass. These changes can be correlated with structural rearrangements upon poling. Following sodium departure linked to Q^1 phosphate groups, charge compensation is done by the formation of additional P-O-P linkages. The role of fluorine ions departure on the structural change is more complex and conclusions could not be unraveled, since fluorine can be present in different anionic units bonded to phosphorus or the other ions present in glass matrix. Therefore, the question remains open and future work is necessary to comprehend the role of fluorine drift and its impact on the chemical reactivity of the glass surface for

instance since the oxide layer is expected to show different resistance to water as compared to the oxyfluoride “virgin” glass.

4. CONCLUSION

In this work, the use of thermal poling in fluorophosphate glass as an imprinting process to induce optical modification has been demonstrated. It was described not only cationic migration towards anode (sodium in our case), but also fluorine anionic migration towards cathode from the glass network occurs upon poling treatment, forming a controlled oxide richer layer under the glass surface in contact with the anode compared to the original glass. The distribution of sodium and fluorine in the glass were analyzed and revealed that a 180 nm layer with less sodium and fluorine was created. It has been shown that using micro-structured electrodes it was possible to faithfully transfer the electrode pattern to the glass poled surface through the electrostatic imprint process during poling treatment. Topological changes have been also observed with a surface variation of -60 nm of amplitude and the phase contrast image analysis has allowed evidencing that a positive *n* variation of 0.06. These results open huge perspectives for implementing flat micro-optical components under the fluorophosphate glass surface with high refractive index contrast by controlling cations and anions migrations.

Acknowledgments

Authors would like to acknowledge the Brazilian funding agencies FAPESP - Fundação de Amparo à Pesquisa do Estado de São Paulo (Project N. 2013/07793-6, CEPID program); CAPES - Coordenação de Aperfeiçoamento de Pessoal de Nível Superior; CNPq - Conselho Nacional de Desenvolvimento Científico e Tecnológico (Universal project 130562/2018-1). GG personally acknowledges funding by FAPESP grant 2019/12442-4 for a postdoctoral fellowship.

References

[1] M. Dussauze, T. Cremoux, F. Adamietz, V. Rodriguez, E. Fargin, G. Yang, T. Cardinal, Thermal Poling of Optical Glasses: Mechanisms and Second-Order Optical Properties, Int J Appl Glass Sci. 3 (2012) 309–320. https://doi.org/10.1111/ijag.12001.

[2] A. Delestre, M. Lahaye, E. Fargin, M. Bellec, A. Royon, L. Canioni, M. Dussauze, F. Adamietz, V. Rodriguez, Towards second-harmonic generation micropatterning of glass surface, Appl Phys Lett. (2010). https://doi.org/10.1063/1.3350895.

[3] M. Dussauze, E. Fargin, A. Malakho, V. Rodriguez, T. Buffeteau, F. Adamietz, Correlation of large SHG responses with structural characterization in borophosphate niobium glasses, Opt Mater (Amst). 28 (2006) 1417–1422. https://doi.org/10.1016/j.optmat.2005.08.026.
[4] G. Guimbretìre, M. Dussauze, V. Rodriguez, E.I. Kamitsos, Correlation between second-order optical response and structure in thermally poled sodium niobium-germanate glass, Appl Phys Lett. (2010). https://doi.org/10.1063/1.3506501.
[5] M. Dussauze, E. Fargin, V. Rodriguez, A. Malakho, E. Kamitsos, Enhanced Raman scattering in thermally poled sodium-niobium borophosphate glasses, J Appl Phys. 101 (2007). https://doi.org/10.1063/1.2724798.
[6] A.G. Clare, A.C. Wright, R.N. Sinclair, A Comparison of the structural role of Na+ network modifying cations in sodium silicate and sodium fluoroberyllate glasses, J Non Cryst Solids. 213–214 (1997) 321–324. https://doi.org/10.1016/S0022-3093(97)00015-X.
[7] A. von Hippel, E.P. Gross, J.G. Jelatis, M. Geller, Photocurrent, space-charge buildup, and field emission in alkali halide crystals, Physical Review. 91 (1953). https://doi.org/10.1103/PhysRev.91.568.
[8] Y. Luo, A. Biswas, A. Frauenglass, S.R.J. Brueck, Large second-harmonic signal in thermally poled lead glass-silica waveguides, Appl Phys Lett. (2004). https://doi.org/10.1063/1.1760213.
[9] A. Malakho, E. Fargin, A. Delestre, C. Andŕ, T. Cardinal, M. Lahaye, V. Rodriguez, M. Couzi, F. Adamietz, L. Canioni, A. Royon, Second-harmonic generation in sodium and niobium borophosphate glasses after poling under field-assisted silver ions anodic injection, J Appl Phys. 104 (2008). https://doi.org/10.1063/1.2973156.
[10] G. Poirier, M. Dussauze, V. Rodriguez, F. Adamietz, L. Karam, T. Cardinal, E. Fargin, Second Harmonic Generation in Sodium Tantalum Germanate Glasses by Thermal Poling, Journal of Physical Chemistry C. 123 (2019) 26528–26535. https://doi.org/10.1021/acs.jpcc.9b08221.
[11] M. Dussauze, V. Rodriguez, F. Adamietz, G. Yang, F. Bondu, A. Lepicard, M. Chafer, T. Cardinal, E. Fargin, Accurate Second Harmonic Generation Microimprinting in Glassy Oxide Materials, Adv Opt Mater. 4 (2016) 929–935. https://doi.org/10.1002/adom.201500759.
[12] A. Lipovskii, V. Zhurikhina, D. Tagantsev, 2D-structuring of glasses via thermal poling: A short review, Int J Appl Glass Sci. (2017). https://doi.org/10.1111/ijag.12273.
[13] F. Lind, D. Palles, D. Möncke, E.I. Kamitsos, L. Wondraczek, Modifying the surface wetting behavior of soda-lime silicate glass substrates through thermal poling, J Non Cryst Solids. (2017). https://doi.org/10.1016/j.jnoncrysol.2017.02.006.
[14] L. Karam, F. Adamietz, V. Rodriguez, F. Bondu, A. Lepicard, T. Cardinal, E. Fargin, K. Richardson, M. Dussauze, The effect of the sodium content on the structure and the optical properties of thermally poled sodium and niobium borophosphate glasses, J Appl Phys. 128 (2020) 043106. https://doi.org/10.1063/5.0013383.
[15] A.L.R. Brennand, J.S. Wilkinson, Planar waveguides in multicomponent glasses fabricated by field-driven differential drift of cations, Opt Lett. (2007). https://doi.org/10.1364/ol.27.000906.
[16] R. Alvarado, L. Karam, R. Dahmani, A. Lepicard, F. Calzavara, A. Piarristeguy, A. Pradel, T. Cardinal, F. Adamietz, E. Fargin, M. Chazot, K. Richardson, L. Vellutini, M. Dussauze, Patterning of the Surface Electrical Potential on Chalcogenide Glasses by a Thermoelectrical Imprinting Process, The Journal of Physical Chemistry C. 124 (2020) 23150–23157. https://doi.org/10.1021/acs.jpcc.0c06507.
[17] A. Lepicard, T. Cardinal, E. Fargin, F. Adamietz, V. Rodriguez, K. Richardson, M. Dussauze, Micro-structuring the surface reactivity of a borosilicate glass via thermal poling, Chem Phys Lett. (2016). https://doi.org/10.1016/j.cplett.2016.09.077.
[18] A. Lepicard, F. Bondu, M. Kang, L. Sisken, A. Yadav, F. Adamietz, V. Rodriguez, K. Richardson, M. Dussauze, Long-lived monolithic micro-optics for multispectral GRIN applications, Sci Rep. 8 (2018). https://doi.org/10.1038/s41598-018-25481-x.
[19] M. Dussauze, V. Rodriguez, F. Adamietz, F. Bondu, A. Lepicard, T. Cardinal, E. Fargin, Spatial

and geometry control of second order optical properties in inorganic amorphous materials, in: 2016. https://doi.org/10.1364/bgpp.2016.bt5b.4.
[20] V. Janicki, I. Fabijanić, P. Pervan, B. Okorn, J. Sancho-Parramon, Ellipsometry-based study of poled glass refractive index depth profiles, in: Optics InfoBase Conference Papers, 2019. https://doi.org/10.1364/OIC.2019.ThA.8.
[21] R.A. Myers, N. Mukherjee, S.R.J. Brueck, Large second-order nonlinearity in poled fused silica, Opt Lett. (2008). https://doi.org/10.1364/ol.16.001732.
[22] D. Raskhodchikov, I. Reshetov, P. Brunkov, V. Kaasik, A. Lipovskii, D. Tagantsev, Mechanism of Thermal Charge Relaxation in Poled Silicate Glasses in a Wide Temperature Range (From Liquid Nitrogen to Glass Melting Temperature), Journal of Physical Chemistry B. 124 (2020) 7948–7956. https://doi.org/10.1021/acs.jpcb.0c04537.
[23] A. v. Redkov, V.G. Melehin, A.A. Lipovskii, How Does Thermal Poling Produce Interstitial Molecular Oxygen in Silicate Glasses?, Journal of Physical Chemistry C. 119 (2015) 17298–17307. https://doi.org/10.1021/acs.jpcc.5b04513.
[24] M. Dussauze, E.I. Kamitsos, E. Fargin, V. Rodriguez, Structural rearrangements and second-order optical response in the space charge layer of thermally poled sodium-niobium borophosphate glasses, Journal of Physical Chemistry C. (2007). https://doi.org/10.1021/jp074335f.
[25] B. Ferreira, E. Fargin, B. Guillaume, G. le Flem, V. Rodriguez, M. Couzi, T. Buffeteau, L. Canioni, L. Sarger, G. Martinelli, Y. Quiquempois, H. Zeghlache, L. Carpentier, Second harmonic generation in poled tellurite glass, J Non Cryst Solids. 332 (2003) 207–218. https://doi.org/10.1016/j.jnoncrysol.2003.09.015.
[26] A. Narazaki, K. Tanaka, K. Hirao, N. Soga, Effect of poling temperature on optical second harmonic intensity of sodium zinc tellurite glasses, J Appl Phys. 83 (1998) 3986–3990. https://doi.org/10.1063/1.367154.
[27] H. Guo, X. Zheng, M. Lu, K. Zou, B. Peng, S. Gu, H. Liu, X. Zhao, Large second-order nonlinearity in thermally poled Ge-Sb-Cd-S chalcogenide glass, Opt Mater (Amst). (2009). https://doi.org/10.1016/j.optmat.2008.10.044.
[28] M. Dussauze, X. Zheng, V. Rodriguez, E. Fargin, T. Cardinal, F. Smektala, Photosensitivity and second harmonic generation in chalcogenide arsenic sulfide poled glasses, Opt Mater Express. (2011). https://doi.org/10.1364/ome.2.000045.
[29] H. Ebendorff-Heidepriem, Fluoride phosphate and phosphate glasses for photonics, Phosphorus Research Bulletin. 13 (2002). https://doi.org/10.3363/prb1992.13.0_11.
[30] X. Zou, K. Itoh, H. Toratani, Transmission loss characteristics of fluorophosphate optical fibers in the ultraviolet to visible wavelength region, J Non Cryst Solids. 215 (1997). https://doi.org/10.1016/S0022-3093(97)00034-3.
[31] E.I. Kamitsos, A.P. Patsis, M.A. Karakassides, G.D. Chryssikos, Infrared reflectance spectra of lithium borate glasses, J Non Cryst Solids. (1990). https://doi.org/10.1016/0022-3093(90)91023-K.
[32] K.V. Krishnaiah, E. Soares de Lima Filho, Y. Ledemi, G. Nemova, Y. Messaddeq, R. Kashyap, Development of ytterbium-doped oxyfluoride glasses for laser cooling applications, Sci Rep. 6 (2016) 21905. https://doi.org/10.1038/srep21905.
[33] G. Galleani, Y. Ledemi, E.S.E.S. de Lima Filho, S. Morency, G. Delaizir, S. Chenu, J.R.J.R. Duclere, Y. Messaddeq, UV-transmitting step-index fluorophosphate glass fiber fabricated by the crucible technique, Opt Mater (Amst). 64 (2017) 524–532. https://doi.org/10.1016/j.optmat.2017.01.017.
[34] P.N. Brunkov, V.G. Melekhin, V. v. Goncharov, A.A. Lipovskii, M.I. Petrov, Submicron-resolved relief formation in poled glasses and glass-metal nanocomposites, Technical Physics Letters. (2008). https://doi.org/10.1134/S1063785008120122.
[35] H. Takagi, S.I. Miyazawa, M. Takahashi, R. Maeda, Electrostatic imprint process for glass,

Applied Physics Express. (2008). https://doi.org/10.1143/APEX.1.024003.
[36] M. Dussauze, E. Fargin, M. Lahaye, V. Rodriguez, F. Adamietz, Large second-harmonic generation of thermally poled sodium borophosphate glasses, Opt Express. 13 (2005) 4064. https://doi.org/10.1364/opex.13.004064.
[37] A. Lepicard, T. Cardinal, E. Fargin, F. Adamietz, V. Rodriguez, K. Richardson, M. Dussauze, Surface Reactivity Control of a Borosilicate Glass Using Thermal Poling, Journal of Physical Chemistry C. (2015). https://doi.org/10.1021/acs.jpcc.5b07139.
[38] X. Zhang, R. Zhang, L. Hu, J. Ren, Precipitation of Er^{3+}-doped $Na_5Y_9F_{32}$ crystals from fluorophosphate glasses: An advanced solid-state NMR spectroscopic study, J Mater Chem C Mater. 7 (2019) 6728–6743. https://doi.org/10.1039/c9tc00256a.
[39] G. Galleani, S.H. Santagneli, Y. Messaddeq, M. de Oliveira, H. Eckert, Rare-earth doped fluoride phosphate glasses: structural foundations of their luminescence properties, Phys. Chem. Chem. Phys. 19 (2017) 21612–21624. https://doi.org/10.1039/C7CP03927A.
[40] G. Galleani, H. Bradtmüller, H. Fares, S.H. Santagneli, M. Nalin, H. Eckert, BiF3Incorporation in Na/Ba Mixed Network Modifier Fluoride-Phosphate Glasses: Structural Studies by Solid-State NMR and Raman Spectroscopies, Journal of Physical Chemistry C. 124 (2020) 25578–25587. https://doi.org/10.1021/acs.jpcc.0c07792.
[41] M. Poulain, M. Poulain, Multicomponent fluoride glasses, J Non Cryst Solids. 213–214 (1997) 40–43. https://doi.org/10.1016/S0022-3093(97)00095-1.
[42] D.E. Brow, R.K., Tallant, D.R., Osborne, Z.A., Yang, Y., Day, Effect of fluorine on the structure of phosphate glass, Physics and Chemistry of Glasses. 32 (1991) 188–195.
[43] V.N. Rai, B.N.R. Sekhar, D.M. Phase, S.K. Deb, Effect of gamma irradiation on the structure and valence state of Nd in phosphate glass, (2014). https://arxiv.org/abs/1406.4686 (accessed September 13, 2021).
[44] T. Djouama, M. Poulain, B. Bureau, R. Lebullenger, Structural investigation of fluorophosphate glasses by 19F, 31P MAS-NMR and IR spectroscopy, J Non Cryst Solids. 414 (2015) 16–20. https://doi.org/10.1016/j.jnoncrysol.2015.01.017.
[45] W. Strojek, H. Eckert, Medium-range order in sodium phosphate glasses: A quantitative rotational echo double resonance solid state NMR study, Physical Chemistry Chemical Physics. 8 (2006) 2276–2285. https://doi.org/10.1039/b518080e.
[46] L. Karam, F. Adamietz, V. Rodriguez, F. Bondu, A. Lepicard, T. Cardinal, E. Fargin, K. Richardson, M. Dussauze, The effect of the sodium content on the structure and the optical properties of thermally poled sodium and niobium borophosphate glasses, J Appl Phys. (2020). https://doi.org/10.1063/5.0013383.
[47] M. Oto, S. Kikugawa, T. Miura, M. Hirano, H. Hosono, Fluorine doped silica glass fiber for deep ultraviolet light, J Non Cryst Solids. 349 (2004) 133–138. https://doi.org/10.1016/j.jnoncrysol.2004.08.220.
[48] M. Oto, Resistivity for deep-UV laser irradiation in fluorine doped silica glass fiber, in: L. Juha, R.H. Sobierajski, H. Wabnitz (Eds.), IEEE Photonics Technology Letters, 2007: pp. 65860N-65860N. https://doi.org/10.1117/12.723972.
[49] K. Tsukuma, N. Yamada, S. Kondo, K. Honda, H. Segawa, Refractive index, dispersion and absorption of fluorine-doped silica glass in the deep UV region, J Non Cryst Solids. 127 (1991) 191–196. https://doi.org/10.1016/0022-3093(91)90142-S.